Front. Optoelectron. 2012, 5(3): 266–270
DOI 10.1007/s12200-012-0253-2

RESEARCH ARTICLE

A simple infrared nanosensor array based on carbon nanoparticles

Junjie DAI, Longyan YUAN, Qize ZHONG, Fengchao ZHANG, Hongfei CHEN, Chao YOU, Xiaohong FAN, Bin HU, Jun ZHOU (✉)

Wuhan National Laboratory for Optoelectronics (WNLO), College of Optoelectronic Science and Engineering, Huazhong University of Science and Technology, Wuhan 430074, China

© Higher Education Press and Springer-Verlag Berlin Heidelberg 2012

Abstract A simple (2×2) pixelated flexible infrared nanosensor array based on carbon nanoparticles (CNPs) was fabricated through a simple and low-cost flame method. By integrated with a micro controller unit, the sensor array could detect power density of incident infrared light in real-time. The mechanism for the superior infrared sensing property of the flexible sensor array based on CNP was also studied in detail in this work.

Keywords carbon nanoparticles (CNPs), infrared sensor, array

1 Introduction

Flexible electronics have attracted increasing attention due to their outstanding applications in portable and wearable consumer electronics [1–5]. Large-scale integration of high-performance electronic components on mechanically flexible substrates may enable new applications in displays, sensor arrays and energy devices [1,6–11]. Infrared sensing is critical to thermal imaging, temperature monitoring, remote sensing and night vision devices, as well as thermal photovoltaic and other industrial applications [9–15]. For the last two decades, intensive efforts have been devoted to develop environmental friendly, infrared sensitive materials [16–19].

Recently, carbon nanoparticles (CNPs) have drawn increasing attention owing to their attractive applications in bio-imaging, optoelectronic devices and infrared devices [20,21]. We have recently fabricated highly flexible infrared nanosensors based on CNPs with the response time of about 68 ms and the maximum photocurrent change of about 52.9% in air at room temperature [6]. In this work, we have fabricated a sensitive infrared nanosensor array based on CNPs and integrated the sensor array with micro controller unit (MCU) to detect infrared power density in real-time.

Received February 7, 2012; accepted June 4, 2012

E-mail: jun.zhou@mail.hust.edu.cn

2 Methods and results

A schematic diagram of the fabrication of flexible infrared sensor array is shown in Fig. 1. Firstly, CNPs were grown on ceramic plate through shadow mask by a simple flame synthesis process (Fig. 1(a)) [6]. Briefly, a common alcohol burner was used to grow CNPs. A ceramic plate covered by a metallic mask with a 2 × 2 array (each pattern has a dimension of 5 mm × 5 mm) was mounted in the flame core of about 5.5 cm above the wick of an alcohol burner. The temperature at the surface of the ceramic plate was about 800°C. The growth process lasted for 30 s to 5 min, and then the ceramic plate was taken out from the flame. Secondly, mixing the polydimethylsiloxane (PDMS) base and curing agent with a ratio of 10∶1 and cured at 60°C for about 15 min to form a pre-cured PDMS substrate. Thirdly, the ceramic plate with CNPs was placed on the pre-cured PDMS with the side that had grown CNPs facing the PDMS substrate. After the PDMS substrate was fully cured, ceramic plate were carefully peeled off from the PDMS substrate (Figs. 1(b) and 1(c)). Figure 1(d) shows the optical image of the fabricated device. Finally, Ti/Ag electrodes were deposited at the two ends of each CNP film through shadow mask, forming a 2 × 2 flexible infrared sensor array.

The morphology and structure of the CNPs were studied by field emission scanning electron microscopy (SEM: FEI Sirion 200) and Renishaw-in Via Raman spectrometer (514.5 nm line of an Ar^+ laser) at room temperature. Figure 1(e) shows the SEM image of the CNPs transferred onto the PDMS substrate. The CNPs are homogeneous and

uniform in particle size. The typical Raman spectrum of CNPs is shown in Fig. 1(f). It can be seen that the G peak at 1601 cm^{-1} and D peak at 1343 cm^{-1} have the highest intensity in the spectrum. The G band reveals that the CNPs grown on ceramic plate contain sp^2 carbon networks, while the D and D′ band are defect-induced Raman features, indicating the CNPs contain some degree of disordering [22,23].

The infrared response of the device was intensively studied by using an Nd:YAG laser (1064 nm), which worked in pulse mode with tunable pulse width and frequency as a light source at room temperature. The pulse width of the laser was fixed at 2 ms. The incident power of the infrared radiation was measured by an Ophir NOVA power meter. The photoresponse of the device was recorded by a low-noise current preamplifier (Stanford Research systems model SR570) and a synthesized function generator (Stanford Research systems model DS345). Figure 2(a) shows the typical photocurrent (by substract the dark current) response of pixel 1 of the array which was characterized by recording the current change under a fixed bias of 5 V with different incident infrared power densities. The dependence of the photocurrent on the incident infrared power density demonstrates a linear relationship as expected (Fig. 2(b)).

The performance of the infrared nanosensor array to detect the infrared light power density was characterized by the MCU system including analog to digital converter (ADC), digital display tubes and matching resistances (Fig. 3(a)). The incident of the laser on each pixel of the infrared nanosensor array can contribute to the change of the pixel's resistance that is then compared to the matched resistance to obtain the change of the output voltage. After that, this signal was sent to the MCU system after pasting through ADC to obtain the output signal, aiming at driving the digital displays that showed the infrared light power density of the original laser beam. In our test, we defined level 1 to demonstrate the pixel's photocurrent of 15.6 nA under the infrared light density of 1.37 $mW/mm^{2.}$ The same principle can be used in the rest. Level 2, 3, 4, 5 can separately and independently demonstrate for the photocurrent of 23.1, 43.2, 52.0 and 66.4 nA under the infrared light density of 2.17, 2.67, 3.38, and 5.2 mW/mm^2, which are shown in Fig. 2(a).

Then, the infrared beam was focused on each pixel at a power density of 3.38 mW/mm^2 and the photocurrents of all the four pixels were recorded, as shown in Fig. 3(b). It can be observed that the pixels had the highest photo-

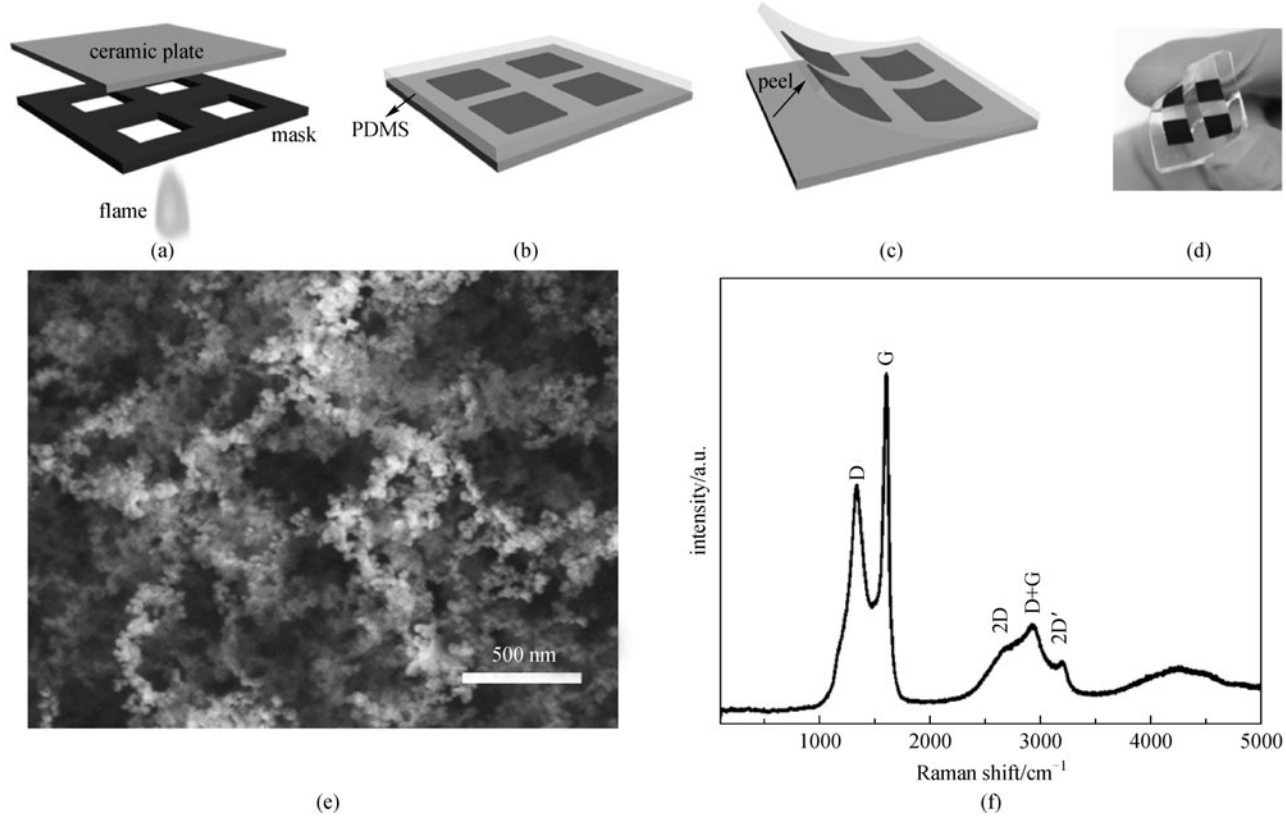

Fig. 1 Schematic diagram of fabrication of flexible infrared sensor array. (a) Experimental setup for the growth of CNPs on ceramic plate; (b) ceramic plate with CNPs on it was placed onto pre-cured PDMS substrate; (c) CNPs were transferred to PDMS substrate by peeling ceramic plate from PDMS; (d) optical image for fabricated device; (e) SEM image of CNPs on PDMS; (f) Raman spectrum of CNPs

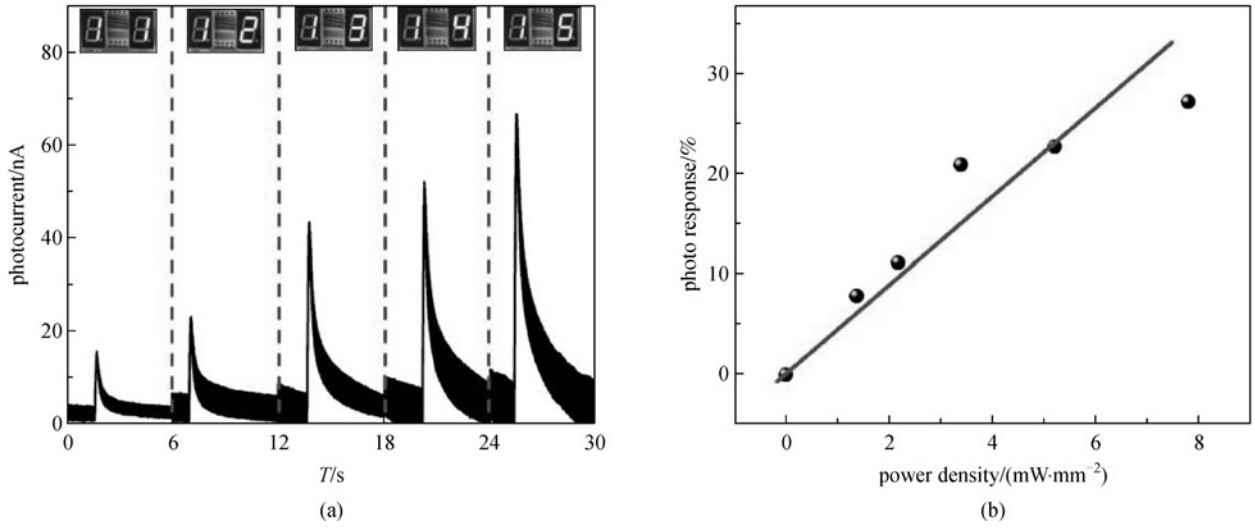

Fig. 2 (a) Photocurrent response of pixel 1 of device at different power density of 2.17, 2.67, 3.38 and 5.2 mW/mm^2, respectively. The upper insets showed the measured power level received by pixel 1; (b) dependence of photocurrent of pixel 1 of device at different power densities. The dots and line show the experimental data and the corresponding fitting curve, respectively

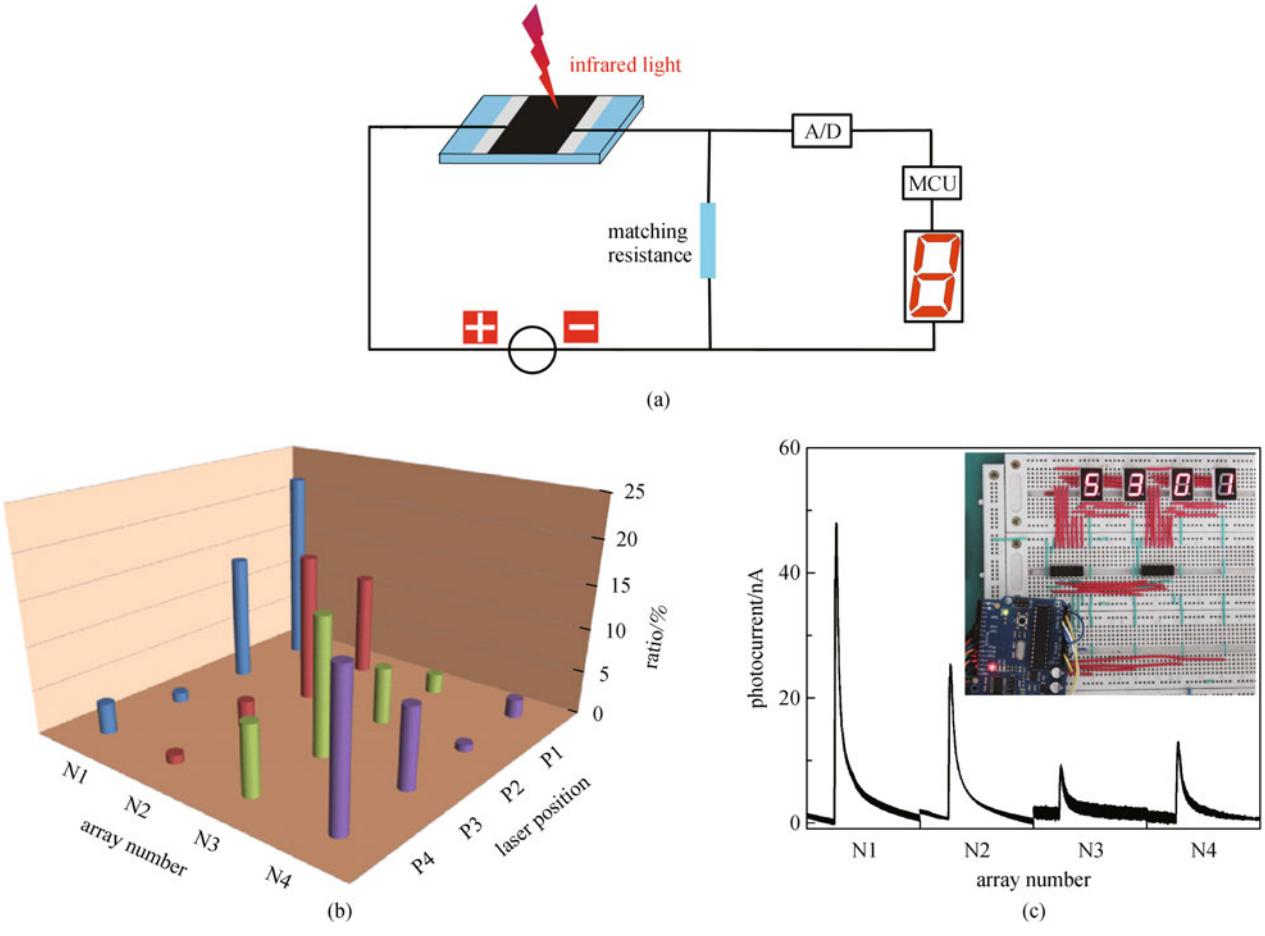

Fig. 3 (a) Schematic diagram of measurement system; (b) relationship between photoresponse of each pixel of infrared sensor array and pixel spot on which the laser beam was focused; (c) photocurrent response of four different pixels of photosensor array as laser beam was focused on pixel 1. The inset shows four digital numbers of 5, 3, 0 and 1, demonstrating the level of the power densities received by pixels 1, 2, 3 and 4, respectively

current response when the incident infrared light focused on it, while the other three ones showed weaker response. To demonstrate our sensor array can be used to detect the intensity of the incident light, a simple demo was shown here. Figure 3(c) revealed the photoresponse of the all four pixels when the infrared beam was focus on pixel 1. Pixel 1 received the highest infrared power, and pixel 2 and 4 had a lower one, while pixel 3 received the lowest power, resulting from their relative position with incident infrared light. In the meanwhile, we could obtain digital numbers of 5, 3, 0, 1, which showed the intensities of incident infrared on pixel 1, 2, 3 and 4 (inset in Fig. 3(c)). Thus, on the basis of our previous definition, we could derive the original infrared light power and photocurrent of each pixel from the number showing by the digital displays.

3 Discussion

We are trying to introduce the exciton model to explain the infrared response of our devices based on CNPs [17–19]. In our experiment, the amount of excitons generated in CNPs increased with the infrared power density they received, contributing to a large photocurrent since the excitons are dissociated to electron-hole pairs by electrical field or/and thermal [18], which was shown in Fig. 2(a). In addition, the thermal insulated PDMS substrate [6] could inhibit fast thermal dissipation without exciton excitation and preserved more thermal energy to produce excitons in CNPs, thus increase the photocurrent response of the fabricated infrared sensors. In a word, the optoelectronic characteristics of CNPs and the thermal insulating substrate benefit for the superior photoresponse of the fabricated infrared sensor.

In summary, we developed a novel infrared nanosensor array on flexible substrate based on CNPs via a simple flame method. The linear relationship between the photocurrent response and infrared power density assured its usage in real-time infrared power detection. The simple and low-cost fabrication procedure for the infrared nanosensor array could be easily scaled up for large-scale products yielding. This work fulfills the objective to promising route for the fabrication of low-cost, multi-pixels infrared nanosensor array with potential practical application.

Acknowledgements J. Zhou thanks for the financial support of the project from the National Natural Science Foundation of China (Grant No. 51002056), the National Basic Research Program of China (No. 2012CB619302), the Foundation for the Author of National Excellent Doctoral Dissertation of China (No. 201035), the Program for New Century Excellent Talents in University (NCET-10-0397). L. Y. Yuan thanks the support from the China Postdoctoral Science Foundation (No. 20100480892). J. J. Dai thanks the support from the graduate innovation fund of Huazhong University of Science and Technology (HF-09-19-2011-230). The authors thank the Analysis and Testing Center of Huazhong University of Science and Technology for support.

References

1. Takei K, Takahashi T, Ho J C, Ko H, Gillies A G, Leu P W, Fearing R S, Javey A. Nanowire active-matrix circuitry for low-voltage macroscale artificial skin. Nature Materials, 2010, 9(10): 821–826
2. Sekitani T, Noguchi Y, Hata K, Fukushima T, Aida T, Someya T. A rubberlike stretchable active matrix using elastic conductors. Science, 2008, 321(5895): 1468–1472
3. Ko H C, Stoykovich M P, Song J Z, Malyarchuk V, Choi W M, Yu C J, Geddes J B 3rd, Xiao J L, Wang S D, Huang Y G, Rogers J A. A hemispherical electronic eye camera based on compressible silicon optoelectronics. Nature, 2008, 454(7205): 748–753
4. Sekitani T, Yokota T, Zschieschang U, Klauk H, Bauer S, Takeuchi K, Takamiya M, Sakurai T, Someya T. Organic nonvolatile memory transistors for flexible sensor arrays. Science, 2009, 326(5959): 1516–1519
5. Yamada T, Hayamizu Y, Yamamoto Y, Yomogida Y, Izadi-Najafabadi A, Futaba D N, Hata K. A stretchable carbon nanotube strain sensor for human-motion detection. Nature Nanotechnology, 2011, 6(5): 296–301
6. Yuan L Y, Dai J J, Fan X H, Song T, Tao Y T, Wang K, Xu Z, Zhang J, Bai X D, Lu P X, Chen J, Zhou J, Wang Z L. Self-cleaning flexible infrared nanosensor based on carbon nanoparticles. ACS Nano, 2011, 5(5): 4007–4013
7. Xiao X, Yuan L, Zhong J, Ding T, Liu Y, Cai Z, Rong Y, Han H, Zhou J, Wang Z L. High-strain sensors based on ZnO nanowire/polystyrene hybridized flexible films. Advanced Materials, 2011, 23 (45): 5440–5444
8. Yuan L Y, Tao Y T, Chen J, Dai J J, Song T, Ruan M Y, Ma Z W, Gong L, Liu K, Zhang X H, Hu X J, Zhou J, Wang Z L. Carbon nanoparticles on carbon fabric for flexible and high-performance field emitters. Advanced Functional Materials, 2011, 21(11): 2150–2154
9. McDonald S A, Konstantatos G, Zhang S G, Cyr P W, Klem E J D, Levina L, Sargent E H. Solution-processed PbS quantum dot infrared photodetectors and photovoltaics. Nature Materials, 2005, 4 (2): 138–142
10. Johnston K W, Pattantyus-Abraham A G, Clifford J P, Myrskog S H, MacNeil D D, Levina L, Sargent E H. Schottky-quantum dot photovoltaics for efficient infrared power conversion. Applied Physics Letters, 2008, 92(15): 151115
11. Klem E J D, MacNeil D D, Levina L, Sargent E H. Solution processed photovoltaic devices with 2% infrared monochromatic power conversion efficiency: performance optimization and oxide formation. Advanced Materials, 2008, 20(18): 3433–3439
12. Xiao L, Zhang Y Y, Wang Y, Liu K, Wang Z, Li T Y, Jiang Z, Shi J P, Liu L A, Li Q Q, Zhao Y G, Feng Z H, Fan S S, Jiang K L. A polarized infrared thermal detector made from super-aligned multiwalled carbon nanotube films. Nanotechnology, 2011, 22(2): 025502
13. Rauch T, Boberl M, Tedde S F, Furst J, Kovalenko M V, Hesser G N, Lemmer U, Heiss W, Hayden O. Near-infrared imaging with quantum-dot-sensitized organic photodiodes. Nature Photonics, 2009, 3(6): 332–336
14. Schödel R, Ott T, Genzel R, Hofmann R, Lehnert M, Eckart A,

Mouawad N, Alexander T, Reid M J, Lenzen R, Hartung M, Lacombe F, Rouan D, Gendron E, Rousset G, Lagrange A M, Brandner W, Ageorges N, Lidman C, Moorwood A F M, Spyromilio J, Hubin N, Menten K M. A star in a 15.2-year orbit around the supermassive black hole at the centre of the Milky Way. Nature, 2002, 419(6908): 694–696

15. Xu F L, Liu X, Fujimura K. Pedestrian detection and tracking with night vision. IEEE Transactions on Intelligent Transportation Systems, 2005, 6(1): 63–71
16. Bachilo S M, Strano M S, Kittrell C, Hauge R H, Smalley R E, Weisman R B. Structure-assigned optical spectra of single-walled carbon nanotubes. Science, 2002, 298(5602): 2361–2366
17. Freitag M, Martin Y, Misewich J A, Martel R, Avouris P H. Photoconductivity of single carbon nanotubes. Nano Letters, 2003, 3(8): 1067–1071
18. Itkis M E, Borondics F, Yu A P, Haddon R C. Bolometric infrared photoresponse of suspended single-walled carbon nanotube films. Science, 2006, 312(5772): 413–416
19. Pradhan B, Setyowati K, Liu H Y, Waldeck D H, Chen J. Carbon nanotube-polymer nanocomposite infrared sensor. Nano Letters, 2008, 8(4): 1142–1146
20. Liu H P, Ye T, Mao C D. Fluorescent carbon nanoparticles derived from candle soot. Angewandte Chemie International Edition, 2007, 46(34): 6473–6475
21. Yang S T, Cao L, Luo P G J, Lu F S, Wang X, Wang H F, Meziani M J, Liu Y F, Qi G, Sun Y P. Carbon dots for optical imaging in vivo. Journal of the American Chemical Society, 2009, 131(32): 11308–11309
22. Ferrari A C, Meyer J C, Scardaci V, Casiraghi C, Lazzeri M, Mauri F, Piscanec S, Jiang D, Novoselov K S, Roth S, Geim A K. Raman spectrum of graphene and graphene layers. Physical Review Letters, 2006, 97(18): 187401
23. Pimenta M A, Dresselhaus G, Dresselhaus M S, Cançado L G, Jorio A, Saito R. Studying disorder in graphite-based systems by Raman spectroscopy. Physical Chemistry Chemical Physics, 2007, 9(11): 1276–1291